

LiCuS, an intermediate phase in the electrochemical conversion reaction of CuS with Li: A potential environment-friendly battery and solar cell material



Andreea Beleanu^a, Janos Kiss^a, Michael Baenitz^a, Mayukh Majumder^a, Anatoliy Senyshyn^b, Guido Kreiner^a, Claudia Felser^{a,*}

^a Max-Planck-Institut für Chemische Physik fester Stoffe, Nöthnitzer Strasse 40, 01187 Dresden, Germany

^b Anatoliy Senyshyn, Heinz Maier-Leibnitz Zentrum, Lichtenberstrasse 1, 85747 Garching, Germany

ARTICLE INFO

Article history:

Received 8 January 2016
Received in revised form
16 February 2016
Accepted 17 February 2016
Available online 19 February 2016

Keywords:

Li-ion batteries
Crystal structure
DFT calculations
Optoelectronics
New materials
NMR

ABSTRACT

The crystal structure of a ternary sulfide with the approximate composition LiCuS, which is a promising candidate for environment-friendly battery and solar cell materials is reported. The crystal structure was solved by a combination of neutron and X-ray powder diffraction data, and ⁷Li solid-state NMR analysis. A yellow powder, Li_{1.1}Cu_{0.9}S, was obtained by the reaction of CuS with a slight excess of Li metal. The compound crystallizes in the Na₃AgO₂ structure type in the space group *Ibam*. An idealized crystal structure of Li_{1.1}Cu_{0.9}S can be derived from the cubic Li₂S structure by moving a part of the Li along the *c* axis so that these Li atoms become linearly coordinated by S. All the metal sites are occupied by randomly mixed Li and Cu atoms; however, there is a strong preference for linear coordination by Cu. The density functional theory calculations show that Li_{1.1}Cu_{0.9}S is a direct band-gap semiconductor with an energy gap of 1.95 eV in agreement with experimental data.

© 2016 The Authors. Published by Elsevier Masson SAS. This is an open access article under the CC BY-NC-ND license (<http://creativecommons.org/licenses/by-nc-nd/4.0/>).

1. Introduction

Nowadays, Li-ion batteries are playing a major role in mobile electronics applications, and are produced in an industrial scale for mobile phones, laptops, and other gadgets. In the near future, it is expected that electric cars will run on Li-ion batteries instead of fossil fuels, and large-capacity Li-ion accumulators will provide temporary storage for renewable energy applications such as solar cells and wind turbines. Therefore, Li-based compounds have widely been investigated in order to obtain new electrode materials for all types of battery systems: primary, secondary, or rechargeable batteries [1–6].

The Li–S battery system has been investigated for several decades because its high theoretical specific energy density is much greater than that of conventional Li-ion batteries [7]. An alternate class of cathode materials is 3*d*-transition-metal sulfides because they retain high capacities and reversibility even after prolonged charge-discharge cycling. Although a large number of compounds

are now studied, there is an immense interest in developing alternative materials with higher energy densities at lower costs [8,9]. For example, Cu₂S is not only a promising cathode material but is also very attractive for various applications such as optoelectronic devices [10,11], solar cells [12,13], and other types of batteries [14]. CuS is specifically interesting because of its high specific capacity and good electronic conductivity [15–17]. The latter compound and the corresponding electrochemical conversion reaction mechanism, CuS + 2Li = Li₂S + Cu, have been investigated several times in the past [18–30] and recently by X-ray diffraction (XRD) and solid-state NMR spectroscopy [18]. It has been found that the electrochemical conversion reaction of CuS with Li is rather complex and involves the formation of an intermediate phase, Li_{*x*}CuS, with *x* close to 1. CuS inserts a small amount of Li in the first step of the process, forming the terminal solid-solution phase, Li_{*x*}CuS, with *x* ≤ 0.16. Then, the latter reacts with more Li to afford the intermediate phase, Li₁CuS. Li₂S has been observed to form in significant amounts together with small amounts of Cu particles starting from *x* = 0.85. Therefore, the second step of lithiation is expressed by the reaction, LiCuS + Li = Li₂S + Cu. A small amount of Cu_{1.96}S has been found in fully discharged samples, which was explained by the decomposition of Li₁CuS [18].

* Corresponding author.

E-mail address: claudia.felser@cpfs.mpg.de (C. Felser).

A detailed study of the thermal and electrochemical behavior of $\text{Cu}_{4-x}\text{Li}_x\text{S}_2$ ($x = 1, 2, 3$) phases has been reported in Ref. [30]. In this work it was shown that Cu_3LiS_2 ($x = 1$) and LiCuS ($x = 2$) crystallize with unique crystal structures of low symmetry at room temperature. It was not possible to solve the crystal structures but both phases undergo a structural transformation at above 140 °C. The compounds are then isostructural with the end members Cu_2S and Li_2S [30].

Recently, it was suggested that LiCuS is a suitable substitute for the CdS buffer layer in conventional chalcopyrite-based thin-film solar cells [31]. CdS is harmful to the environment and expensive; therefore, there is a strong demand for alternative buffer-layer materials [32]. Thin films of LiCuS have been prepared by radio-frequency sputtering using a target with a 1:1:1 molar ratio of Li, Cu, and S. A target with a brownish surface has been obtained by hot sintering fine powders of Cu_2S and Li_2S at ~870 K and 22 MPa. The sputtered films on glass were transparent with a yellow color, corresponding to an energy band gap between 2.0 and 2.5 eV. Unfortunately, it was not possible to analyze the exact composition of the film; however, the composition may be close to the intermediate phase of the CuS/Li electrochemical conversion process.

The main objective of this work was the bulk synthesis of the yellow phase close to the composition, LiCuS , and to determine its chemical composition and crystal structure by powder diffraction techniques and ^7Li solid-state NMR spectroscopy.

2. Experimental

Polycrystalline $\text{Li}_{1.1}\text{Cu}_{0.9}\text{S}$ was obtained by the reaction of Li foil (99.999%) with CuS powder (anhydrous, 99.999%) both from Sigma Aldrich, close to 1:1 stoichiometry, but with a slight excess of Li. A mixture of the starting materials was pressed into pellets and placed in Al_2O_3 tubes (\varnothing 14 mm, Al23, Friatec). The total mass was ~1 g per sample. Each crucible was enclosed by an evacuated and with 300 mbar Ar backfilled fused silica ampoule. All handling was performed in a glove-box in Ar atmosphere (Braun, pO_2 , $\text{pH}_2\text{O} < 1$ ppm) as protecting atmosphere. The heat treatment was as follows: After increasing the temperature of the mixture to 723 K at a heating rate of 1 K/min, the temperature was held at 723 K for 96 h and then reduced to room temperature at a cooling rate of 1 K/min. After the reaction, a yellow, air- and moisture-sensitive powder was obtained. The optical microscopy revealed small Cu particles as a second phase. The sample was characterized using powder X-ray diffraction ($3^\circ < 2\theta < 100^\circ$, Huber Guinier camera 670, $\text{Cu K}\alpha_1$ radiation, $\lambda = 1.54051$ Å, transmission geometry, Ge monochromator, flat sample holder with Kapton foil). Refinement of the lattice parameter: LaB_6 as internal standard (SRM660a, $a = 4.156916$ Å).

In addition elastic coherent neutron scattering experiments were performed on the high-resolution powder diffractometer, SPODI, at the neutron research reactor FRM II (Garching, Germany) [33]. Monochromatic neutrons (1.54832(2) Å) were obtained at a 155° take-off angle using the (551) reflection of a vertically focused composite Ge monochromator. The two-dimensional powder diffraction data were collected at 4 and 293 K and then corrected for geometric aberrations and curvature of the Debye-Scherrer rings as described in Ref. [33]. The measurements performed at 293 and 4 K reveal that the sample remained isostructural in this temperature range. The powder patterns were indexed using Werner's algorithm [34]. The crystal structure was solved with Expo2013 [35] and refined using Jana2006 [36]. Details on the crystal structure investigations may be obtained from the Fachinformationszentrum Karlsruhe, 7344 Eggenstein-Leopoldshafen, Germany (fax: (+49)7247-808-666; email: crysdata@fiz-karlsruhe.de), on quoting the depository numbers CSD-427746

(4 K) and CSD-427747 (293 K). See also the Supporting information.

The intensity vs. 2θ plots of the observed and calculated neutron powder diffraction patterns are shown in Fig. S1 and S2 in Supporting Information. The ^7Li NMR (nuclear spin $I = 3/2$) measurements were performed in a fixed field of 2.734 T in a Janis 9 T cryostat at 4.2 K using a Tecmag pulse NMR spectrometer. The pulsed NMR spin echo $90-180^\circ$ sequence was applied. A 5 μs pulse was used to excite the entire spectra, and $\tau = 10$ s repetition time was used to accumulate the spin echo because of the long nuclear spin-lattice relaxation time of the semiconducting material at low temperatures. The Fourier transform of the spin echo in time domain provides the NMR line as a function of frequency.

To gain more insight into the electronic structure of $\text{Li}_{1.1}\text{Cu}_{0.9}\text{S}$, we carried out density functional theory (DFT) calculations by employing the fully-relativistic Korringa-Kohn-Rostoker (KKR) Green's function method, as implemented in the SPR-KKR package [37]. For considering the disorder due to the random occupation of the atomic sites in $\text{Li}_{1.1}\text{Cu}_{0.9}\text{S}$, we used the single-site coherent potential approximation (CPA) [38,39] which is a rather efficient mean-field technique. The electronic exchange and correlation interactions were treated within the PBE [40] version of the generalized-gradient approximation (GGA). In the calculations, we used the experimental atomic structure and site occupations.

3. Results and discussion

3.1. Synthesis

The polycrystalline material of the yellow phase was obtained by reducing CuS with Li metal according to the following chemical reaction: $\text{CuS} + 1.1 \text{Li} = \text{Li}_{1.1}\text{Cu}_{0.9}\text{S} + 0.1 \text{Cu}$. It was possible to observe the elemental Cu as small particles using an optical microscope. Moreover, the Bragg reflections of Cu are clearly distinguished from that of the main phase in the X-ray and neutron powder diffraction patterns. The refined phase fraction (5 wt% Cu) is also in good agreement with the fraction (7 wt%) calculated from the refined composition $\text{Li}_{1.10}\text{Cu}_{0.90}\text{S}$. The inductively coupled plasma optical emission spectrometry (ICP-OES) chemical analysis show a composition of $\text{Li}_{1.17(3)}\text{Cu}_{1.07(3)}\text{S}$ for the product mixture. Finally, the formation of Li_2S according to the chemical reaction, $\text{LiCuS} + \text{Li} = \text{Li}_2\text{S} + \text{Cu}$, was not observed. One Bragg reflection of a low intensity (see the first Bragg reflection of the powder patterns at $2\theta = 14.3^\circ$ in Figs. S1 and S2 in Supporting Information) could not be assigned to either the title compound or elemental Cu. This peak originates from a new phase ($\ll 1$ wt%) with dark gray or black color and probably forms in the CuS/Li electrochemical conversion process with slightly less Li content than the title compound. The mixtures of the yellow and the black phase and some $(\text{Li,Cu})_2\text{S}$ could be obtained after the heat treatment at 500 °C for 1 week from Cu_2S and Li_2S mixtures in various ratios. Thus, all the experimental data support the off-stoichiometric formation of the yellow phase without perceptible homogeneity range. The title compound is extremely moisture and air sensitive. After a short time in the glovebox, the yellow powder becomes brownish at the surface. The powder patterns of such samples show additional Bragg reflections.

3.2. Crystal structure

The compound crystallizes orthorhombic with Na_3AgO_2 crystal structure type ($\text{Li}_{1.1}\text{Cu}_{0.9}\text{S}$, $M_r = 96.89$, neutrons, powder, orthorhombic, $Ibam$, $a = 5.632(1)$ Å, $b = 11.209(3)$ Å, $c = 5.982(2)$ Å, $V = 377.6(2)$ Å³ (293 K), $\rho_{\text{calc}} = 3.4051$ gcm⁻³, $R_p = 0.0279$, $R_{\text{fall}} = 0.0606$). The crystal data and Rietveld refinements results for $\text{Li}_{1.1}\text{Cu}_{0.9}\text{S}$ and Cu are listed in Table S1. The atomic coordinates and isotropic displacement parameters at 4 and 293 K are listed in

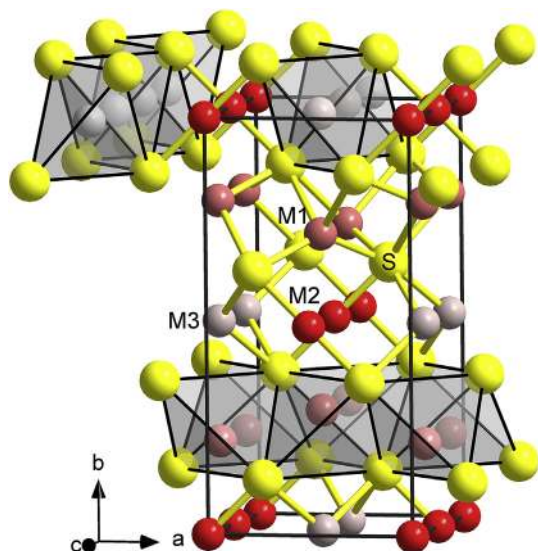


Fig. 1. Crystal structure of $\text{Li}_{1.1}\text{Cu}_{0.9}\text{S}$. The metal sites, M, are occupied by randomly mixed Li and Cu atoms. The M1 site shows a slight site-occupation preference for Li atoms ($\text{Cu}_{0.41}, \text{Li}_{0.59}$). The M2 ($\text{Cu}_{0.88}, \text{Li}_{0.12}$) and M3 ($\text{Cu}_{0.09}, \text{Li}_{0.91}$) sites show a strong preferential site occupation for Cu and Li atoms, respectively.

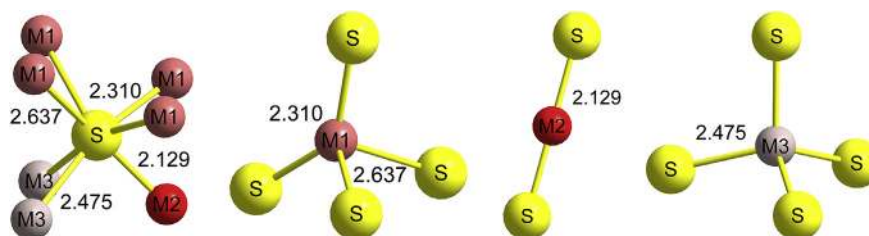


Fig. 2. Atomic environments for the four different crystallographic sites of $\text{Li}_{1.1}\text{Cu}_{0.9}\text{S}$ at 293 K. Distances are given in Å.

Tables S2 and S3, and the interatomic distances are listed in Table S4 in Supporting Information. The crystal structure is shown in Fig. 1, and the coordination-type polyhedra are shown in Fig. 2. There are 24 atoms per unit cell, occupying four different crystallographic sites. S occupies 8j (S), and the remaining metals, Li and Cu, occupy 8g (M1), 4c (M2), and 4b (M3). All the metals sites are occupied by randomly mixed Li and Cu atoms.

Each site has been checked for disorder by a separate refinement without constrains. Then, in the final cycles of the refinement all metal sites has been constrained to a value of one for each site occupation factor. The M1 site shows a slight site-occupation

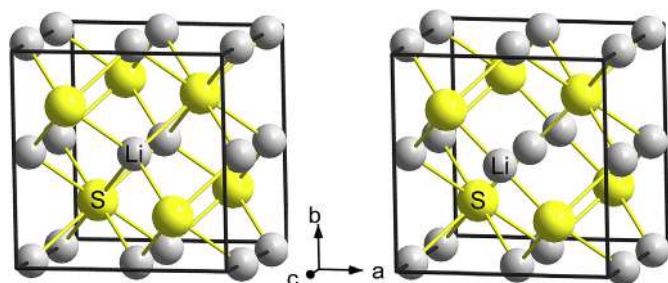


Fig. 3. (left) Crystal structure of Li_2S ($a = 5.716 \text{ \AA}$, $Fm\text{-}3m$, anti- CaF_2 structure type) in unconventional setting emphasizing the atomic environment of S. (right) Hypothetical crystal structure of Li_2S ($P4_2/mcm$), showing the same structural features of $\text{Li}_{1.1}\text{Cu}_{0.9}\text{S}$. The structure was obtained by moving Li from sites $\frac{1}{2}, \frac{1}{2}, \frac{1}{4}$ to $\frac{1}{2}, \frac{1}{2}, 0$.

preference for Li atoms ($\text{Cu}_{0.41}, \text{Li}_{0.59}$), whereas the M2 ($\text{Cu}_{0.88}, \text{Li}_{0.12}$) and M3 ($\text{Cu}_{0.09}, \text{Li}_{0.91}$) sites show a strong preference for Cu and Li atoms, respectively. Thus, the crystal structure of $\text{Li}_{1.1}\text{Cu}_{0.9}\text{S}$ is a disordered variant of the crystal structure of Li_3AuS_2 [41]. In the latter structure the sites 4b and 8g are fully occupied by Li atoms and the 4c site by Au atoms.

The S atoms are surrounded by seven metal atoms ($\text{SLi}_{2.7}\text{Cu}_{4.3}$). Its coordination-type polyhedron can be derived from a distorted cube. Herein, one edge of the cube was omitted, and the two corresponding metal atoms were replaced by an atom (M2) located at the midpoint of the former cube edge. The distances, S–M, range from 2.129 Å to 2.637 Å. The coordination-type polyhedron of M1 is a distorted M1S_4 tetrahedron with the M1–S distances, 2.310 Å and 2.637 Å. The M2 site forms a dipole, i.e., it is linearly coordinated by two S atoms (M2S_2), and the distance, M2–S, is 2.129 Å.

Such a distance is rather short, but still physically reasonable. Distances in the range 2.1–2.2 Å have been reported for several phases with fully occupied sites for Li–S as well as for Cu–S in the Pearson's Crystal Data Bank [42]. An example for Li is the crystal structure of $\text{Li}_4\text{Re}_6\text{S}_{11}$ [43] with a distance Li–S = 2.09 Å and an example for Cu is Cu_5NaS_3 with a distance of Cu–S = 2.19 Å [44]. The sum of the effective ionic radii according to Shannon [45] for Cu^+ (0.6 Å, CN = 2) and S^{2-} (1.7 Å, CN = 6) is 2.3 Å. A reliable radius for Li^+ with coordination number 2 is not reported. However, it is

justified to use for Li^+ with coordination number 2 the same radius as for Cu^+ because the radii for coordination number 4 are similar (0.73 Å for Li^+ and 0.74 for Cu^+). The shortest distance (2.13 Å) in

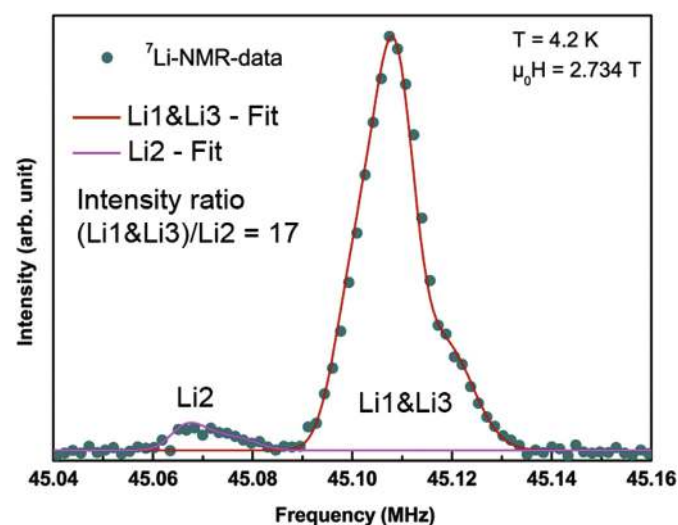


Fig. 4. ^7Li solid-state NMR of $\text{Li}_{1.1}\text{Cu}_{0.9}\text{S}$. The two well-separated lines are assigned to Li2 with linear coordination by S and Li1, Li3, both tetrahedrally coordinated by S. Both the lines show a sizeable chemical shift anisotropy typical for the tetragonal symmetry.

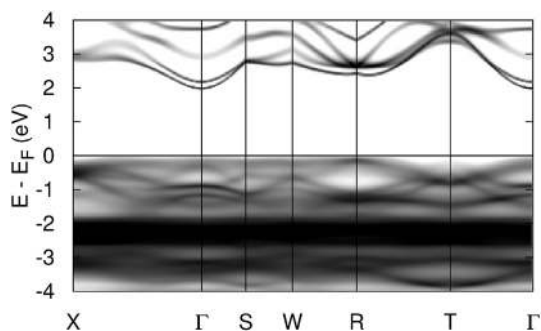


Fig. 5. Band structure of $\text{Li}_{1.1}\text{Cu}_{0.9}\text{S}$ calculated using the PBE functional and CPA alloy theory.

the crystal structure of $\text{Li}_{1.1}\text{Cu}_{0.9}\text{S}$ is then about 7% shorter than the sum of the ionic radii. The unit cell volume of $\text{Li}_{1.1}\text{Cu}_{0.9}\text{S}$ was contracted by $\sim 1.4\%$ at 4 K compared to that at room temperature. However, the short distance, $M2-S$, remains constant within error margins in this temperature range, while longer distances become significantly smaller (Table S4). This indicates that a distance between 2.1 Å and 2.2 Å is a lower limit for the contacts between Cu, Li, and S. The coordination polyhedron of the $M3$ site is a nearly regular $M3S_4$ tetrahedron with $d(M3-S) = 2.475$ Å.

The crystal structure can be described as an alternate stacking of two different types of layers along the b axis as shown in Fig. 1. The first layer is composed of $M1S_{4/4}$ tetrahedra, which are joined via four of their edges. The resulting composition of this layer is $(\text{Cu}_{0.41}, \text{Li}_{0.59})\text{S}$. This type of edge-sharing layer is known from the structure of red PbO with O at the tetrahedron centers and Pb at the vertices. The Li_2S structure with anti- CaF_2 structure type is a three-dimensional network of edge-sharing LiS_4 tetrahedra, i.e., the structure was obtained by stacking $\text{LiS}_{4/4}$ layers along the remaining direction. The second type of layer was obtained by connecting the linear chains of composition $(\text{Cu}_{0.09}, \text{Li}_{0.91})\text{S}_{4/2}$ via linearly coordinated $M2$ ($\text{Cu}_{0.88}, \text{Li}_{0.12}$). The chains were formed by $M3S_4$ tetrahedra, which are linked via opposite edges. These tetrahedra share edges with the tetrahedra of the $M1S_{4/4}$ layers.

An idealized crystal structure of $\text{Li}_{1.1}\text{Cu}_{0.9}\text{S}$ can be derived from the cubic Li_2S structure with $a = 5.716$ Å as shown in Fig. 3. On the left side, a unit cell of the Li_2S structure with anti- CaF_2 structure type is shown in an unconventional setting, highlighting the arrangement of the SLi_8 cubes. Moving the central chain of Li atoms by $1/4c$, i.e., the Li atom at the crystallographic site $\frac{1}{2}, \frac{1}{2}, \frac{1}{4}$ moves to $\frac{1}{2}, \frac{1}{2}, 0$ results in a crystal structure with $P4_2/mcm$ symmetry. This idealized structure shows already all the important features of the structure of $\text{Li}_{1.1}\text{Cu}_{0.9}\text{S}$. The S atoms have coordination number 7. Two Li atoms per unit cell are linearly coordinated by S such as $M2$, and the two remaining Li positions are tetrahedrally coordinated by S, comparable to $M1$ and $M3$. Then, the doubling of the b axis to $2b$ and a body-centered arrangement allow the distances of the structure to be optimized with respect to the chemical composition. This was achieved by puckering the metal atoms ($M1$) in the a - c plane and by a slight change in the unit cell parameters.

The ^7Li solid-state NMR spectrum of polycrystalline $\text{Li}_{1.1}\text{Cu}_{0.9}\text{S}$, as shown in Fig. 4, can be fitted by two well-separated lines with a sizeable chemical shift anisotropy, typical for a tetragonal symmetry. The two lines indicate two different types of atomic environment for the Li atoms. The peak with a lower intensity can be assigned to the linearly coordinated $\text{Li}2$ species, and the large peak can be assigned to $\text{Li}1$ and $\text{Li}3$, which are both tetrahedrally surrounded by S. This assignment is based on the NMR intensity ratio, which should be equal to the ratio of Li atoms in linear and tetrahedral coordination modes. The intensity ratio, 17, was slightly

larger than the number ratio, 10. However, one should keep in mind that the error of the intensity ratio is expected to be large due to the small intensity contribution of the $\text{Li}2$ line. Notably, ^7Li has nuclear spin $3/2$, which can result in a quadrupolar interaction if the crystal structure is noncubic. However, no satellites were detected, which is probably caused by too small a quadrupolar interaction, forcing the satellites to merge with the central transition. The ^7Li solid-state NMR spectrum of polycrystalline $\text{Li}_{1.1}\text{Cu}_{0.9}\text{S}$ is compared to that of cubic Li_2S in Fig. S3 in Supporting Information.

3.3. DFT calculations

The Bloch-spectral function (BSF) of $\text{Li}_{1.1}\text{Cu}_{0.9}\text{S}$ is shown in Fig. 5. The data obtained show that $\text{Li}_{1.1}\text{Cu}_{0.9}\text{S}$ is a direct band-gap semiconductor with an energy band gap (at Γ point) of 1.95 eV, and the indirect energy band gap in the vicinity of the R point is 2.55 eV. This is in very good agreement with the 2.0 and 2.5 eV optical direct and indirect band gaps measured for the radio-frequency sputter deposited $\text{Li}_{x-1}\text{Cu}_x\text{S}$ thin film on quartz glass [31]. The calculated BSF indicates that because of the (Li,Cu) disorder in $\text{Li}_{1.1}\text{Cu}_{0.9}\text{S}$, the bands close to the top of the valence band were rather flat, showing little dispersion. Due to the strong disorder on the Li and Cu sites the valence bands are rather smeared compared to an ordered compound.

4. Conclusion

In summary, the crystal structure of the yellow intermediate phase of the CuS/Li electrochemical conversion process shows off-stoichiometric formation without perceptible homogeneity range. The crystal structure is a disordered variant of the Na_3AgO_2 structure type. All the metal sites are occupied by randomly mixed Cu and Li atoms, which are linearly and tetrahedrally coordinated by S atoms. The crystal structure is closely related to that of Li_2S . The main features of the crystal structure may be derived by moving a part of the Li chains in such a manner that the atoms change their environment from tetrahedral to linear coordination by S. These sites show a strong site-occupation preference for Cu. $\text{Li}_{1.1}\text{Cu}_{0.9}\text{S}$ is extremely moisture and air sensitive and a direct band-gap semiconductor with a band gap of 1.95 eV, thus causing the yellow color. There is strong evidence that at a slightly lower Li content, a further intermediate phase of black color is formed in the CuS/Li electrochemical conversion process, thus making the process even more complex.

Acknowledgements

We would like to thank Steffen Hückmann, Kathrin Hofmann, Barbara Albert for X-ray diffraction measurements, Gudrun Auf-fermann, Ulrike Schmidt, Anja Völzke and Sebastian Schwinger for chemical analyses and Rainer Pöttgen for valuable comments. Financial support from the ERC Grant (291472) is gratefully acknowledged.

Appendix A. Supplementary data

Supplementary data related to this article can be found at <http://dx.doi.org/10.1016/j.solidstatesciences.2016.02.010>.

References

- [1] P.G. Bruce, *Chem. Commun.* 19 (1997) 1817.
- [2] D. Guyomard, J.M. Tarascon, *Solid State Ionics* 69 (1994) 222.
- [3] R. Koksang, J. Barker, H. Shi, M.Y. Saidi, *Solid State Ionics* 84 (1996) 1.
- [4] M. Winter, J.O. Besenhard, M.E. Spahr, P. Novak, *Adv. Mater.* 10 (1998) 725.
- [5] J.M. Tarascon, M. Armand, *Nature* 414 (2001) 359.

- [6] B. Ammundsen, J. Paulsen, *Adv. Mater.* 13 (2001) 943.
- [7] M. Armand, J.-M. Tarascon, *Nature* 451 (2008) 652.
- [8] F. Yongzhu, A. Manthiram, *Electrochim. Acta* 109 (2013) 716.
- [9] F. Bonino, M. Lazzari, B. Rivolta, B. Scrosati, *J. Electrochem. Soc.* 131 (1984) 1498.
- [10] Y. Lou, X.B. Chen, C.J. Samia, A.C. Burda, *J. Phys. Chem. B* 107 (2003) 12431.
- [11] H.T. Zhang, G. Wu, X.H. Chen, *Langmuir* 21 (2005) 4281.
- [12] H. Lee, S.W. Yoon, E.J. Kim, J. Park, *J. Nano Lett.* 7 (2007) 778.
- [13] N.S. Xu, S.E. Huq, *Mater. Sci. Eng. R.* 48 (2005) 47.
- [14] J. Chen, S.Z. Deng, N.S. Xu, S.H. Wang, X.G. Wen, S.H. Yang, C.L. Yang, J.N. Wang, W.K. Ge, *Appl. Phys. Lett.* 80 (2002) 3620.
- [15] K. Okamoto, S. Kawai, *Jpn. J. Appl. Phys.* 12 (1973) 1130.
- [16] A. Etienne, *J. Electrochem. Soc.* 117 (1970) 870.
- [17] N. Margalit (Ed.), *Proceedings of the Symposium on Battery Design and Optimization of the Electrochemical Society*, Princeton, New Jersey, 1979, p. 320.
- [18] N. Yamakawa, M. Jiang, C.P. Grey, *Chem. Mater.* 21 (2009) 3162.
- [19] A. Attewell, P. Tattershall (Eds.), *Proceedings of the 29th Power Sources Symposium of the Electrochemical Society*, Pennington, New Jersey, 1980, p. 53.
- [20] L.W. Langrish (Ed.), *Proceedings of the 29th Power Sources Symposium of the PSC Publication Committee* Red Bank, New Jersey, 1969, p. 67.
- [21] D. Linden, N. Wilburn, E. Brooks (Eds.), *Proceedings of the 8th International Power Sources Symposium*, Paper No. 20, Brighton, 1972, p. 58.
- [22] R.J. Jasinski, *J. Electroanal. Chem. Interf. Electrochem.* 26 (1970) 189.
- [23] J.P. Gabano, V.L. Décheneaux, G.M. Gerbier, J. Jammet, *J. Electrochem. Soc.* 119 (1972) 459.
- [24] A.J. Cuesta, D.D. Bump (Eds.), *Proceedings of the Symposia on Power Sources on Biomedical Implantable Applications and Ambient Temperature Lithium Batteries*, The Electrochemical Society Princeton, New Jersey, 1980, p. 95.
- [25] A.M. Bredland, T.G. Messing, J.W. Paulson (Eds.), *Proceedings of the 29th Power Sources Symposium of the Electrochemical Society* Pennington, New Jersey, 1980, p. 82.
- [26] J.S. Chung, H.J. Sohn, *J. Power Sources* 108 (2002) 226.
- [27] F.W. Dampier, *J. Electrochem. Soc.* 121 (1974) 656.
- [28] G. Eichinger, H.P. Fritz, *Electrochim. Acta* 20 (1975) 753.
- [29] G. Eichinger, J.O. Besenhard, *J. Electroanal. Chem.* 72 (1976) 1.
- [30] E.M. Chen, P.F.P. Poudeu, *J. Solid State Chem.* 232 (2015) 8.
- [31] D. Kieven, A. Grimm, A. Beleanu, C.G.F. Blum, J. Schmidt, T. Rissom, I. Laueremann, T. Gruhn, C. Felser, R. Klenk, *Thin Solid Films* 519 (2011) 1866.
- [32] D. Kieven, R. Klenk, S. Naghavi, C. Felser, T. Gruhn, *Phys. Rev. B* 81 (2010) 075208.
- [33] M. Hoelzel, A. Senyshyn, N. Juenke, H. Boysen, W. Schmahl, H. Fuess, High-resolution neutron powder diffractometer SPODI at research reactor FRM II, *Nucl. Instrum. Methods Phys. Res. Sect. A Accel. Spectrom. Detect. Assoc. Equip.* 667 (2012) 32.
- [34] Treor, Implemented in the Software Package WINXPOW, STOE & CIE GmbH, 2007.
- [35] A. Altomare, C. Cuocci, C. Giacovazzo, A. Moliterni, R. Rizzi, N. Corriero, A. Falcicchio, *J. Appl. Cryst.* 46 (2013) 1231.
- [36] V. Petricek, M. Dusek, L. Palatinus, Jana, *The Crystallographic Computing System*, Institut of Physics, Praha, Czech Republic, 2006.
- [37] H. Ebert, D. Ködderitzsch, J. Minár, *Rep. Prog. Phys.* 74 (2011) 096501.
- [38] P. Soven, *Phys. Rev.* 156 (1967) 809.
- [39] W.H. Butler, *Phys. Rev. B* 31 (1985) 3260.
- [40] J.P. Perdew, K. Burke, M. Ernzerhof, *Phys. Rev. Lett.* 77 (1996) 3865.
- [41] F. Qiang Huang, Y. Yang, C. Flaschenriem, J.A. Ibers, *Inorg. Chem.* 40 (2001) 1397.
- [42] P. Villars, K. Cenzual, *Pearson's Crystal Data – Crystal Structure Data Base for Inorganic Compounds*, Release 2012/2013, ASM International, Materials Park, Ohio, USA.
- [43] W. Bronger, H.J. Miessen, P. Müller, R. Neugröschel, *J. Less-Comm. Met.* 105 (1985) 303.
- [44] H.S. Effenberger, F. Pertlik, *Monatsh. Chem.* 116 (1985) 921.
- [45] R.D. Shannon, *Acta Crystallogr. A* 32 (1976) 751.